Frontiers of Information Technology & Electronic Engineering
www.jzus.zju.edu.cn; engineering.cae.cn; www.springerlink.com
ISSN 2095-9184 (print); ISSN 2095-9230 (online)
E-mail: jzus@zju.edu.cn

Effective degree of freedom for near-field plane-based XL-MIMO with tri-polarization*

Zhe WANG[†1,2], Jiayi ZHANG[†‡1], Wenhui YI[1], Huahua XIAO[3], Dusit NIYATO[2], Bo AI[1]

[1]*School of Electronic and Information Engineering, Beijing Jiaotong University, Beijing 100044, China*

[2]*College of Computing and Data Science, Nanyang Technological University, 639798, Singapore*

[3]*State Key Laboratory of Mobile Network and Mobile Multimedia Technology, ZTE Corporation, Shenzhen 518057, China*

[†]E-mail: zhewang_77@bjtu.edu.cn; jiayizhang@bjtu.edu.cn

Received Mar. 7, 2024; Revision accepted Aug. 8, 2024; Crosschecked

Abstract: This paper considers the effective degree of freedom (EDoF) for extremely large-scale multiple-input-multiple-output (XL-MIMO) systems. We consider two XL-MIMO hardware designs: uniform planar array (UPA)-based and continuous aperture (CAP)-based XL-MIMO as well as two representative near-field channel models: scalar Green's function-based and dyadic Green's function with triple polarization-based near-field channels. First, for UPA-based XL-MIMO a discrete array aperture, we evaluate the EDoF performance by applying discrete channel matrices generated by the scalar or dyadic Green's channel model. Then, for CAP-based XL-MIMO, a tailored EDoF performance evaluation framework for a two-dimensional (2D) CAP plane-based system is constructed by leveraging asymptotic analysis and extending the analysis approaches for a one-dimensional (1D) CAP line segment-based system. This framework incorporates the triple polarized auto-correlation kernel function, which can efficiently capture the impact of multiple polarization on the EDoF performance. Numerical results show that, with an increase in the number of antennas, the UPA-based XL-MIMO system can achieve an EDoF performance close to the EDoF performance for the CAP plane-based XL-MIMO system. Moreover, the EDoF performance can be enhanced by the multiple polarization in channels and increased physical sizes of the transceiver.

unedited

Key words: XL-MIMO; near-field communication; EDoF; polarization effect
https://doi.org/10.1631/FITEE.2400167 **CLC number:**

1 Introduction

With the rapid development of wireless communications, the anticipated evolution beyond fifth-generation (B5G) and sixth-generation (6G) of wireless communication networks have been widely studied (Zhang et al., 2020; Tataria et al., 2021; You et al., 2021; Zhang et al., 2023). Concurrently, the escalation in communication demands and the variety of application scenarios have introduced substantial challenges (Huang et al., 2021; Ouyang et al., 2022; Du et al., 2023; Zheng et al., 2023; Sun et al., 2024). To tackle these challenges, many promising enabled technologies have been widely applied in wireless communication (Letaief et al., 2019; Chen et al.,

‡ Corresponding author

* This project was supported in part by National Natural Science Foundation of China under Grant 62221001, in part by Natural Science Foundation of Jiangsu Province, Major Project under Grant BK20212002, in part by the Fundamental Research Funds for the Central Universities under Grant 2022JBQY004, in part by ZTE Industry-University-Institute Cooperation Funds under Grant No. IA20240319002 & No. IA20240709018, in part by the National Research Foundation, Singapore, and Infocomm Media Development Authority under its Future Communications Research & Development Programme, in part by Defence Science Organisation (DSO) National Laboratories under the AI Singapore Programme (FCP-NTU-RG-2022-010 and FCP-ASTAR-TG-2022-003), in part by Singapore Ministry of Education (MOE) Tier 1 (RG87/22), and in part by the NTU Centre for Computational Technologies in Finance (NTU-CCTF).

© Zhejiang University Press 2024

2021; Zhang et al., 2021b; Du et al., 2024; Gong et al., 2024; Shi et al., 2024; Wang et al., 2024). Among these technologies, extremely large-scale multiple-input-multiple-output (XL-MIMO) technology holds high expectations (Cui et al., 2023; Lu et al., 2024; Lei et al., 2024a; Liu et al., 2024b; Wang et al., 2024).

MIMO technology has been viewed as an important enabler of wireless communication networks since fourth-generation (4G) of wireless communication networks (Marzetta, 2010; Björnson et al., 2019; Gan et al., 2021; Zhang et al., 2021a; Chen et al., 2023; Björnson et al., 2024). As an evolution of conventional massive MIMO (mMIMO) technology, XL-MIMO employs an extremely large number of antennas, for example thousands, even tens of thousands, of antennas (Xu et al., 2023; Lu et al., 2024; Wang et al., 2024). The extremely large array aperture in XL-MIMO necessitates the consideration of near-field spherical wave characteristics, which are typically neglected in conventional mMIMO due to the small or moderate array aperture (You et al., 2023; Liu et al., 2024; Liu et al., 2024c; Wang et al., 2024; Xu et al., 2024). Mainly three promising XL-MIMO hardware designs, e.g. uniform linear array (ULA)-based (Cui and Dai, 2022), uniform planar array (UPA)-based (Lu and Zeng, 2022), and continuous aperture (CAP)-based XL-MIMO designs (Zhang and Dai, 2023), have attracted significant attention (Liu et al., 2024a; Wang et al., 2024; Wang et al., 2024).

To fully explore the benefits of XL-MIMO technology, the performance limit analysis for XL-MIMO systems is vital. Several works have studied the degree of freedom (DoF) for near-field XL-MIMO systems (Yuan et al., 2022; Jiang and Gao, 2023; Ouyang et al., 2023; Xie et al., 2023). Ouyang et al. (2023) reviewed three DoF-related performance metrics and compared their characteristics and insights, and provide important guidelines for DoF performance analysis for near-field XL-MIMO systems. Among the various performance metrics, the effective DoF (EDoF) has garnered significant research interest. The EDoF is an approximate mathematical solution for the number of dominant singular values of the channel (Ouyang et al., 2023). Note that the EDoF can be directly related to the slope of the capacity performance of systems, which is intuitive in depicting the capacity performance. Based on the scalar Green's function-based channel model (we called it as scalar Green channel model in the following briefly), the authors in Xie et al. (2023) and Jiang and Gao (2023) studied the EDoF for both the ULA-based and one-dimensional (1D) CAP line segment systems. Notably, the EDoF expressions in Xie et al. (2023) were computed in novel closed-form. Moreover, the authors in Yuan et al. (2022) analyzed the EDoF performance for the UPA systems with dyadic Green's function-based channel model. Note that the dyadic Green's function captures triple (tri-) polarization, which is more accurate for describing near-field electromagnetic (EM) characteristics compared with the scalar Green channel model (we called it as dyadic Green channel model in the following briefly). However, existing research on the EDoF analysis of CAP systems has been limited to scenarios involving the 1D CAP line segment.

In practice, two-dimensional (2D) plane-based XL-MIMO systems are extensively researched and advocated (Wang et al., 2024). The UPA-based system with the discrete array aperture and the 2D CAP plane-based system with the continuous array aperture are regarded as two promising plane-based XL-MIMO hardware designs. It is crucial to assess the EDoF performance of these designs and explore their respective performance limits. Note that the CAP plane-based system can be regarded as a special case of the UPA-based system by considering an infinite number of antennas while maintaining the same array size. However, the performance analysis frameworks for the CAP and UPA-based systems are carried out in the continuous integral dimension and the discrete matrix dimension (Ouyang et al., 2023), respectively. Conducting further studies to analyze the EDoF performance of 2D CAP plane systems and comparing their performance with UPA systems is both interesting and essential.

To address the research gap, in this study, we analyze the EDoF performance of both UPA-based and 2D CAP plane-based XL-MIMO systems with both the scalar and dyadic Green channels. For UPA-based XL-MIMO, we evaluate the EDoF performance by leveraging the discrete channel matrices for both the scalar Green and the dyadic Green channels. Moreover, we propose a novel EDoF performance analysis framework specifically for the 2D CAP plane systems over the dyadic Green channel with the aid of asymptotic analysis for the EDoF performance analysis framework for the UPA sys-

unedited

tem. This framework embraces the auto-correlation kernel with triple polarization considered, capturing the impact of multiple polarization on the EDoF performance. Finally, numerical results provide the performance comparison between the UPA system and 2D CAP plane system and evaluate the effects of the polarization and the physical size of the transceiver.

2 System model

In this section, we introduce the system model of the UPA-based and CAP-based XL-MIMO systems. More specifically, the system features and channel models are discussed.

2.1 UPA-based XL-MIMO

2.1.1 System feature

We first investigate the UPA-based XL-MIMO as illustrated in Fig. 1, where both a transmitter and a receiver are equipped with a UPA with point antenna elements. The transmitting plane lies in the XY plane with its left-bottom point being the origin. The transmitting array consists of M_V antennas per column and M_H antennas per row. Thus, the transmitter is equipped with $M = M_H M_V$ antennas in total. The antenna spacing in the vertical column and horizontal row are $\Delta_{t,V}$ and $\Delta_{t,H}$, respectively, and the vertical and horizontal side lengths for the transmitter are $L_{t,V} = M_V \Delta_{t,V}$ and $L_{t,H} = M_H \Delta_{t,H}$, respectively. For the convenience of analysis, we define the antenna index row-by-row as $m \in \{1, \ldots, M\}$ from left to right and from bottom to top. Thus, the location of the m-th antenna element at the transmitter can be denoted as

$$\mathbf{r}_{t,m} = [o(m)\,\Delta_{t,H}, j(m)\,\Delta_{t,V}, 0]^T \in \mathbb{R}^3, \qquad (1)$$

where $o(m) = \mathrm{mod}(m-1, M_H)$ and $j(m) = \lfloor (m-1)/M_H \rfloor$ are the indices of the horizontal and vertical directions for the m-th antenna element at the transmitter, respectively. Furthermore, V_T denotes the transmitting volume.

Similarly, for the receiver equipped with a UPA, let N_V, $\Delta_{r,V}$ and $L_{r,V} = N_V \Delta_{r,V}$ denote the number of antennas per column, the vertical antenna spacing, and the vertical side length, respectively. Moreover, we denote the number of antennas per row, the horizontal antenna spacing, and the horizontal side length as N_H, $\Delta_{r,H}$ and $L_{r,H} = N_H \Delta_{r,H}$, respectively. The receiver is equipped with $N = N_H N_V$ antennas, which are also indexed row-by-row as $n \in \{1, \ldots, N\}$ based on the same indexing principle as the transmitter. Thus, the location of the n-th antenna element at the receiver can be represented as

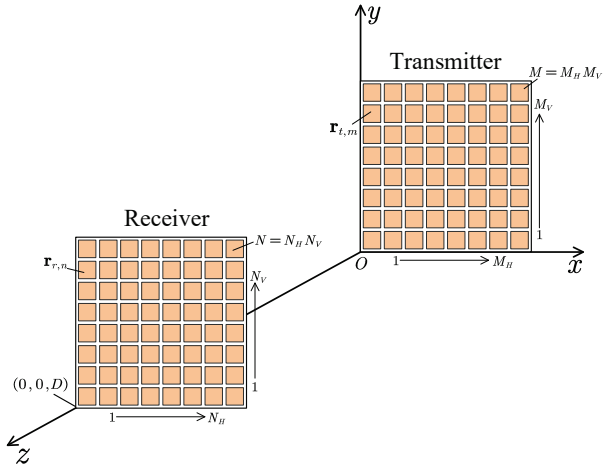

Fig. 1 Illustration of the investigated XL-MIMO system. XL-MIMO, extremely large-scale multiple-input-multiple-output.

$$\mathbf{r}_{r,n} = [t(n)\,\Delta_{r,H}, k(n)\,\Delta_{r,V}, D]^T, \qquad (2)$$

where $t(n) = \mathrm{mod}(n-1, N_H)$ and $k(n) = \lfloor (n-1)/N_H \rfloor$ are the horizontal and vertical indices of the n-th antenna element at the receiver, respectively. Moreover, D is the distance between the left-bottom antenna element of the transmitter and the left-bottom antenna element of the receiver.

2.1.2 Scalar Green channel model

The channel based on the scalar Green's function between a particular receiving point $\mathbf{r}_r \in \mathbb{R}^3$ and a particular transmitting point $\mathbf{r}_t \in \mathbb{R}^3$ can be denoted by (Yuan et al., 2022)

$$G(\mathbf{r}_r, \mathbf{r}_t) = \frac{1}{4\pi} \frac{\exp(-j\kappa_0 |\mathbf{r}_r - \mathbf{r}_t|)}{|\mathbf{r}_r - \mathbf{r}_t|}, \qquad (3)$$

where $\kappa_0 = 2\pi/\lambda$ is the wavenumber and λ is the wavelength. For the UPA-based XL-MIMO system, the channel matrix generated by the scalar Green's function between the receiver with N antennas and the transmitter with M antennas can be denoted as $\mathbf{H}_S \in \mathbb{C}^{N \times M}$, whose (n, m)-th element, $[\mathbf{H}_S]_{nm} = G_{nm}$, is the scalar Green's function between the n-th receiving antenna and m-th transmitting antenna

unedited

defined as (Yuan et al., 2022)

$$G_{nm} = G\left(\mathbf{r}_{r,n}, \mathbf{r}_{t,m}\right) = \frac{1}{4\pi} \frac{\exp\left(-j\kappa_0 d_{nm}\right)}{d_{nm}}, \quad (4)$$

where $\mathbf{r}_{r,n} \in \mathbb{R}^3$ is the location of the n-th receiving antenna, $\mathbf{r}_{t,m} \in \mathbb{R}^3$ is the location of the m-th transmitting antenna, and $d_{nm} = |\mathbf{r}_{r,n} - \mathbf{r}_{t,m}|$ is the distance between the n-th receiving antenna and the m-th transmitting antenna.

2.1.3 Dyadic Green channel model

Note that the scalar Green's function omits the polarization effect, which would have a great effect on the system performance in near-field communications (Yuan et al., 2022; Wei et al., 2023; Wang et al., 2024). To capture full polarization effects, the dyadic Green's function can be applied. More specifically, the dyadic Green's function between a particular receiving point $\mathbf{r}_r \in \mathbb{R}^3$ and a particular transmitting point $\mathbf{r}_t \in \mathbb{R}^3$ can be denoted by $\mathbf{G}\left(\mathbf{r}_r, \mathbf{r}_t\right) \in \mathbb{C}^{3\times 3}$ defined in Eq. (5), where $G\left(\mathbf{r}_r, \mathbf{r}_t\right)$ is the scalar Green's function based channel matrix between $\mathbf{r}_r$ and $\mathbf{r}_t$ given as Eq. (3), $d = |\mathbf{r}_r - \mathbf{r}_t|$ and $\vec{\mathbf{a}}_{rt} = \left(\mathbf{r}_r - \mathbf{r}_t\right) / |\mathbf{r}_r - \mathbf{r}_t|$ is a unit vector describing the direction between $\mathbf{r}_r$ and $\mathbf{r}_t$ (Arnoldus, 2001; Wei et al., 2023; Lei et al., 2024b).

As observed in Eq. (5), the dyadic Green channel $\mathbf{G}\left(\mathbf{r}_r, \mathbf{r}_t\right)$ can be derived by scaling the scalar Green channel $G\left(\mathbf{r}_r, \mathbf{r}_t\right)$ with the operator $(\mathbf{I}_3 + \frac{\nabla_{\mathbf{r}_r} \nabla_{\mathbf{r}_r}^H}{\kappa_0^2})$. An arbitrary dyadic Green's function $\mathbf{G} \in \mathbb{C}^{3\times 3}$ can be written in a matrix form with the (p, q)-th element G^{pq} being the scalar Green's function between the p-th polarization of the receiving point and the q-th polarization of the transmitting source point with $p, q \in \{x, y, z\}$. Thus, the dyadic Green channel between the receiver with N antennas and the transmitter with M antennas can be denoted by $\mathbf{H}_D \in \mathbb{C}^{3N\times 3M}$ as

$$\mathbf{H}_D = \begin{bmatrix} \mathbf{H}^{xx} & \mathbf{H}^{xy} & \mathbf{H}^{xz} \\ \mathbf{H}^{yx} & \mathbf{H}^{yy} & \mathbf{H}^{yz} \\ \mathbf{H}^{zx} & \mathbf{H}^{zy} & \mathbf{H}^{zz} \end{bmatrix}, \quad (6)$$

where $\mathbf{H}^{pq} \in \mathbb{C}^{N\times M}$ is the scalar Green's function channel matrix between the p-th polarization of the receiver with N antennas and the q-th polarization of the transmitter with M antennas. $\mathbf{H}^{pq} \in \mathbb{C}^{N\times M}$ can be further represented in matrix form as

$$\mathbf{H}^{pq} = \begin{bmatrix} G_{11}^{pq} & \cdots & G_{1M}^{pq} \\ \vdots & \ddots & \vdots \\ G_{N1}^{pq} & \cdots & G_{NM}^{pq} \end{bmatrix} \quad (7)$$

where $\left[\mathbf{H}^{pq}\right]_{nm} = G_{nm}^{pq}$ is the (p, q)-th element of the dyadic Green's function between the n-th receiving antenna and the m-th transmitting antenna $\mathbf{G}\left(\mathbf{r}_{r,n}, \mathbf{r}_{t,m}\right)$ as

$$\mathbf{G}\left(\mathbf{r}_{r,n}, \mathbf{r}_{t,m}\right) = \frac{1}{4\pi}\left(\mathbf{I}_3 + \frac{\nabla_{\mathbf{r}_{r,n}} \nabla_{\mathbf{r}_{r,n}}^H}{\kappa_0^2}\right) G\left(\mathbf{r}_{r,n}, \mathbf{r}_{t,m}\right). \quad (8)$$

2.2 CAP plane-based XL-MIMO

2.2.1 System feature

As for the CAP-based XL-MIMO system, we consider a scenario with both a transmitter and a receiver equipped with a 2D CAP plane, where the transmitter is located in the XY plane with its left-bottom point being the origin. Correspondingly, the vertical and horizontal side lengths for the transmitter are $L_{t,V}$ and $L_{t,H}$, respectively. $L_{r,V}$ and $L_{r,H}$ are the vertical and horizontal side lengths for the receiver, respectively. Moreover, the distance between the left-bottom points of the transmitter and the receiver is D. Let S_R and S_T denote the receiving CAP region and the transmitting CAP region, respectively[1].

2.2.2 Green's function-based channel

Note that the 2D CAP planes show continuous features. For the scalar Green channel model, the channel between a particular receiving point $\mathbf{r}_r \in \mathbb{R}^3$ in S_R and a particular transmitting point $\mathbf{r}_t \in \mathbb{R}^3$ in S_T can be denoted by $G\left(\mathbf{r}_r, \mathbf{r}_t\right)$ by substituting respective coordinates into Eq. (3). Moreover, the dyadic Green channel $\mathbf{G}\left(\mathbf{r}_r, \mathbf{r}_t\right) \in \mathbb{C}^{3\times 3}$ for a particular receiving point $\mathbf{r}_r \in \mathbb{R}^3$ in S_R and a particular transmitting point $\mathbf{r}_t \in \mathbb{R}^3$ in S_T can be computed by substituting respective coordinates into Eq. (5).

[1]For the ease of EDoF analysis in the following, we define variables, such as the side length and the locations of transmitting/receiving points similar to that of the UPA system. However, all the analysis frameworks introduced in this paper hold for arbitrary parameter settings instead of limiting the variables in the CAP system similar to that of the UPA system.

unedited

$$\begin{aligned}\mathbf{G}\left(\mathbf{r}_r,\mathbf{r}_t\right)&=\frac{1}{4\pi}\left(\mathbf{I}_3+\frac{\nabla_{\mathbf{r}_r}\nabla_{\mathbf{r}_r}^H}{\kappa_0^2}\right)\frac{\exp\left(-j\kappa_0\left|\mathbf{r}_r-\mathbf{r}_t\right|\right)}{\left|\mathbf{r}_r-\mathbf{r}_t\right|}=\left(\mathbf{I}_3+\frac{\nabla_{\mathbf{r}_r}\nabla_{\mathbf{r}_r}^H}{\kappa_0^2}\right)G\left(\mathbf{r}_r,\mathbf{r}_t\right)\\&=\left(1+\frac{j}{\kappa_0 d}-\frac{1}{\kappa_0^2 d^2}\right)\mathbf{I}_3 G\left(\mathbf{r}_r,\mathbf{r}_t\right)+\left(\frac{3}{\kappa_0^2 d^2}-\frac{3j}{\kappa_0 d}-1\right)\vec{\mathbf{a}}_{rt}\vec{\mathbf{a}}_{rt}^H G\left(\mathbf{r}_r,\mathbf{r}_t\right)\end{aligned}\tag{5}$$

$$\begin{cases}\mathrm{tr}\left(\mathbf{R}_S\right)=\sum_{m=1}^{M}\sum_{n=1}^{N}\left[\mathbf{R}_S\right]_{mm}^2=\sum_{m=1}^{M}\sum_{n=1}^{N}\left|G_{nm}\right|^2\\ \left\|\mathbf{R}_S\right\|_{\mathrm{F}}^2=\sum_{m_1=1}^{M}\sum_{m_2=1}^{N}\left[\mathbf{R}_S\right]_{m_1m_2}^2=\sum_{m_1=1}^{M}\sum_{m_2=1}^{N}\left|\sum_{n=1}^{N}G_{nm_1}^*G_{nm_2}\right|^2\end{cases}\tag{13}$$

3 EDoF analysis

In this section, we construct the EDoF performance analysis framework for the 2D CAP plane systems over both the scalar and dyadic Green channels. To maintain integrity, we first briefly introduce the EDoF analysis framework for the UPA system.

3.1 UPA-based XL-MIMO

3.1.1 Scalar Green channel model

For the UPA system with the scalar Green channel given as Eq. (6), the EDoF ε_S can be approximately computed as Yuan et al. (2022); Ouyang et al. (2023)

$$\varepsilon_S=\frac{\mathrm{tr}^2\left(\mathbf{R}_S\right)}{\left\|\mathbf{R}_S\right\|_{\mathrm{F}}^2},\tag{9}$$

where $\mathbf{R}_S=\mathbf{H}_S^H\mathbf{H}_S\in\mathbb{C}^{M\times M}$ is the correlation matrix for the scalar Green channel.

3.1.2 Dyadic Green channel model

For the dyadic Green channel given in Eq. (6), the EDoF ε_D can be approximated as

$$\varepsilon_D=\frac{\mathrm{tr}^2\left(\mathbf{R}_D\right)}{\left\|\mathbf{R}_D\right\|_{\mathrm{F}}^2},\tag{10}$$

where $\mathbf{R}_D=\mathbf{H}_D^H\mathbf{H}_D\in\mathbb{C}^{3M\times 3M}$ is the correlation matrix for the dyadic Green channel.

3.2 CAP plane-based XL-MIMO

3.2.1 Scalar Green channel model

For CAP plane-based XL-MIMO, the EDoF performance analysis framework, which is different from that of the UPA-based XL-MIMO system, should be implemented due to its continuous array aperture. From the mathematical vision, the CAP plane-based system can be viewed as a special case of the UPA-based system, assuming an infinite number of antennas while maintaining the same physical array size. However, it is not convenient or technically sound to evaluate the EDoF performance for the CAP plane-based system based on the EDoF performance analysis framework for the UPA-based system by considering an infinite number of antennas. This is because the channel matrices would be of infinitely high dimension, leading to extremely high computational complexity, and the EDoF results are also not intuitive for obtaining technical insights for the EDoF performance analysis for the CAP-based system. Thus, it is vital to derive a tailored EDoF performance analysis framework for the CAP-based system. Notably, the auto-correlation kernel $K(\mathbf{r}_t,\mathbf{r}_{t'})$ is defined to indicate the correlation characteristic between two transmitting points in the transmitting region S_T for $\mathbf{r}_t'\in S_T$, $\mathbf{r}_{t'}\in S_T$ over the scalar Green channel as follows (Jiang and Gao, 2023)

$$K(\mathbf{r}_t,\mathbf{r}_{t'})=\int_{S_R}G^*\left(\mathbf{r}_r,\mathbf{r}_t\right)G\left(\mathbf{r}_r,\mathbf{r}_{t'}\right)d\mathbf{r}_r,\tag{11}$$

where $G\left(\mathbf{r}_r,\mathbf{r}_t\right)$ is the scalar Green channel between the transmitting point $\mathbf{r}_t$ and the receiving point $\mathbf{r}_r$. Note that the (m_1,m_2)-th element of the correlation matrix $\mathbf{R}_S$ can be computed as

$$\left[\mathbf{R}_S\right]_{m_1m_2}=\sum_{n=1}^{N}G_{nm_1}^*G_{nm_2},\tag{12}$$

where G_{nm_1} and G_{nm_2} can be calculated as in Eq. (4). Then, $\mathrm{tr}\left(\mathbf{R}_S\right)$ and $\left\|\mathbf{R}_S\right\|_{\mathrm{F}}^2$ in Eq. (9) can be further written in Eq. (13).

Then, by applying the asymptotic analysis for Eq. (13) with the invariant array physical size over $M\to\infty$, $N\to\infty$, $\left[\mathbf{R}_S\right]_{m_1m_2}$, $\mathrm{tr}\left(\mathbf{R}_S\right)$, and $\left\|\mathbf{R}_S\right\|_{\mathrm{F}}^2$

unedited

$$\begin{cases} [\mathbf{R}_S]_{m_1 m_2} \to \frac{N_H N_V}{L_{r,H} L_{r,V}} K(\mathbf{r}_t, \mathbf{r}_{t'}) \\ \mathrm{tr}\left(\mathbf{R}_S\right) \to \frac{N_H N_V M_H M_V}{L_{r,H} L_{r,V} L_{t,H} L_{t,V}} \int_{S_T} \int_{S_R} \left|G\left(\mathbf{r}_r, \mathbf{r}_t\right)\right|^2 d\mathbf{r}_r d\mathbf{r}_t \\ \|\mathbf{R}_S\|_{\mathrm{F}}^2 \to \frac{(N_H N_V M_H M_V)^2}{(L_{r,H} L_{r,V} L_{t,H} L_{t,V})^2} \int_{S_T} \int_{S_T} \left|K(\mathbf{r}_t, \mathbf{r}_{t'})\right|^2 d\mathbf{r}_t d\mathbf{r}_{t'} \end{cases} \tag{14}$$

$$\begin{cases} \mathrm{tr}\left(\mathbf{R}_D\right) = \sum_{c=1}^{3M} [\mathbf{R}_D]_{cc} = \sum_{p=1}^{3} \sum_{i=1}^{3} \sum_{a=1}^{M} \sum_{n=1}^{N} \left|G_{na}^{ip}\right|^2 \\ \|\mathbf{R}_D\|_{\mathrm{F}}^2 = \sum_{c=1}^{3M} \sum_{d=1}^{3M} \left|[\mathbf{R}_D]_{cd}\right|^2 = \sum_{p=1}^{3} \sum_{q=1}^{3} \sum_{a=1}^{M} \sum_{b=1}^{M} \left|\sum_{i=1}^{3} \sum_{n=1}^{N} \left(G_{na}^{ip}\right)^* G_{nb}^{iq}\right|^2 \end{cases} \tag{18}$$

can be asymptotically represented as ub Eq. (14), according to the asymptotic representation (Jiang and Gao, 2023)

$$\begin{cases} d\mathbf{r}_r = dy_r dz_r \to \frac{L_{r,H} L_{r,V}}{N_H N_V} \\ d\mathbf{r}_t = dy_t dz_t \to \frac{L_{t,H} L_{t,V}}{M_H M_V} \\ d\mathbf{r}_{t'} = dy_{t'} dz_{t'} \to \frac{L_{t,H} L_{t,V}}{M_H M_V} \end{cases} \tag{15}$$

Based on the above derivations, the EDoF for the CAP system over the scalar Green channel can be derived as in the following theorem.

Theorem 1 For the CAP-based XL-MIMO system over the scalar Green channel, by applying the asymptotic analysis for Eq. (9) with the invariant array physical size over $M \to \infty$, $N \to \infty$, we can compute the EDoF performance as

$$\Psi_S = \frac{\left(\int_{S_T} \int_{S_R} \left|G\left(\mathbf{r}_r, \mathbf{r}_t\right)\right|^2 d\mathbf{r}_r d\mathbf{r}_t\right)^2}{\int_{S_T} \int_{S_T} \left|K(\mathbf{r}_t, \mathbf{r}_{t'})\right|^2 d\mathbf{r}_t d\mathbf{r}_{t'}}. \tag{16}$$

3.2.2 Dyadic Green channel model

For the CAP system over the dyadic Green channel, motivated by the above analysis of the scalar Green channel model, we also start from the correlation matrix $\mathbf{R}_D$ and dyadic Green channel $\mathbf{H}_D$ for the UPA system.

Relying on the structure of $\mathbf{H}_D$ given in Eq. (6), for the ease of representation, we denote the polarization subscript as $x \to 1$, $y \to 2$, and $z \to 3$, respectively. Based on Eq. (6), the (c, d)-th element of $\mathbf{R}_D \in \mathbb{C}^{3M \times 3M}$ can be constructed as

$$[\mathbf{R}_D]_{cd} = \sum_{i=1}^{3} \sum_{n=1}^{N} \left(G_{na}^{ip}\right)^* G_{nb}^{iq}, \tag{17}$$

where G_{na}^{ip} is the (i, p)-th element of the dyadic Green's function between the n-th receiving antenna and the a-th transmitting antenna $\mathbf{G}\left(\mathbf{r}_{r,n}, \mathbf{r}_{t,a}\right)$ as defined in Eq. (8) with $a = 1, \ldots, M$, $b = 1, \ldots, M$, $\{p, q\} \in \{1, 2, 3\}$, $c = (p-1)M + a$, and $d = (q-1)M + b$, respectively.

Furthermore, $\mathrm{tr}\left(\mathbf{R}_D\right)$ and $\|\mathbf{R}_D\|_{\mathrm{F}}^2$ in Eq. (10) can be expanded as Eq. (18) according to Eq. (17). Note that the diagonal elements of $\mathbf{R}_D$ is derived by letting $c = d$ in $[\mathbf{R}_D]_{cd}$ as

$$(p-1)M + a = (q-1)M + b, \tag{19}$$

which holds only under the conditions $p = q$ and $a = b$. This fact can be easily proven based on the value ranges of these variables. Thus, we can write $\mathrm{tr}\left(\mathbf{R}_D\right)$ as in Eq. (18) by letting $p = q$ and $a = b$ to compute $[\mathbf{R}_D]_{cc}$. Note that the polarization effect can be clearly observed in the expanded form of Eq. (10) as in Eq. (18).

Then, we define the polarized auto-correlation kernel to describe the correlation characteristic between two particular transmitting points in S_T for $\mathbf{r}_t \in S_T$ and $\mathbf{r}_{t'} \in S_T$, over a particular polarization direction pair $\{p, q\} \in \{1, 2, 3\}$

$$\bar{K}(\mathbf{r}_t, \mathbf{r}_{t'}, p, q) = \sum_{i=1}^{3} \int_{S_R} \left[G^{ip}\left(\mathbf{r}_r, \mathbf{r}_t\right)\right]^* G^{iq}\left(\mathbf{r}_r, \mathbf{r}_{t'}\right) d\mathbf{r}_r, \tag{20}$$

where $G^{ip}\left(\mathbf{r}_r, \mathbf{r}_t\right)$ is the (i, p)-th element of the dyadic Green channel between $\mathbf{r}_r \in S_R$ and $\mathbf{r}_t \in S_T$. Compared with the auto-correlation kernel function for the scalar Green channel in Eq. (11), the polarized auto-correlation kernel function in Eq. (20) can capture the polarization effect for a particular polarization direction pair $\{p, q\} \in \{1, 2, 3\}$, which can provide fundamentals for the EDoF performance computation for the CAP system over the dyadic Green channel with polarization.

Under the asymptotic condition $M \to \infty$, $N \to \infty$ with the invariant array physical size, we can obtain the asymptotic form of $\mathrm{tr}\left(\mathbf{R}_D\right)$ and $\|\mathbf{R}_D\|_{\mathrm{F}}^2$ as Eq. (21) by applying the similar asymptotic representations of $d\mathbf{r}_r$, $d\mathbf{r}_t$, and $d\mathbf{r}_{t'}$ as in Eq. (15). As

unedited

$$\begin{cases} \mathrm{tr}\left(\mathbf{R}_D\right) \to \frac{N_H N_V M_H M_V}{L_{r,H} L_{r,V} L_{t,H} L_{t,V}} \sum_{p=1}^{3} \sum_{i=1}^{3} \int_{S_T} \int_{S_R} \left|G^{ip}\left(\mathbf{r}_r, \mathbf{r}_t\right)\right|^2 d\mathbf{r}_r d\mathbf{r}_t \\ \left\|\mathbf{R}_D\right\|_{\mathrm{F}}^2 \to \left(\frac{N_H N_V M_H M_V}{L_{r,H} L_{r,V} L_{t,H} L_{t,V}}\right)^2 \sum_{p=1}^{3} \sum_{q=1}^{3} \int_{S_T} \int_{S_T} \left|\bar{K}(\mathbf{r}_t, \mathbf{r}_{t'}, p, q)\right|^2 d\mathbf{r}_t d\mathbf{r}_{t'} \end{cases} \tag{21}$$

observed in Eq. (21), compared with Eq. (14), the asymptotic representations of $\mathrm{tr}\left(\mathbf{R}_D\right)$ and $\left\|\mathbf{R}_D\right\|_{\mathrm{F}}^2$ capture the polarization effects by considering all possible polarization direction pairs $\{p, q\} \in \{1, 2, 3\}$ with the aid of polarized auto-correlation kernel function defined in Eq. (20).

Thus, based on the above derivations, the EDoF performance for the CAP plane system with the dyadic Green channel can be derived as follows.

Theorem 2 For the CAP plane system based on the dyadic Green channel, by applying the asymptotic analysis for Eq. (9) over $M \to \infty$, $N \to \infty$ with the invariant array physical size, the EDoF can be calculated as

$$\Psi_D = \frac{\left(\sum_{i=1}^{3} \sum_{p=1}^{3} \int_{S_T} \int_{S_R} \left|G^{ip}\left(\mathbf{r}_r, \mathbf{r}_t\right)\right|^2 d\mathbf{r}_r d\mathbf{r}_t\right)^2}{\sum_{p=1}^{3} \sum_{q=1}^{3} \int_{S_T} \int_{S_T} \left|\bar{K}(\mathbf{r}_t, \mathbf{r}_{t'}, p, q)\right|^2 d\mathbf{r}_t d\mathbf{r}_{t'}}. \tag{22}$$

In this section, we provide the EDoF performance analysis frameworks for two plane-based XL-MIMO hardware designs: UPA-based and 2D CAP plane-based systems over two near-field Green's function based channel models: scalar and dyadic Green's function based models. The EDoF performance frameworks in this section are available for the scenario with one transmitting and one receiving plane with any antenna array aperture sizes. The EDoF performance analysis for the scenarios with multiple transmitting or receiving planes is anticipated to be further investigated based on the fundamental frameworks considered in this paper.

4 Numerical results

In this study, we consider the square UPA and 2D CAP plane XL-MIMO systems, where $L_{t,V} = L_{t,H}$ and $L_{r,V} = L_{r,H}$. The number of antennas per side length in the UPA is equal, that is $M_V = M_H$ and $N_V = N_H$. For ease of representation, let L_t and L_r denote the side lengths of the transmitting plane and the receiving plane, respectively. The carrier frequency is 3 GHz.

Figure 2 investigates the EDoF performance for the UPA system versus the number of antennas per side with different side length values. As observed, with the increase in the number of antennas, the EDoF performance would first increase and then reach an approximated saturated performance. Moreover, for a fixed transmitting distance, increasing the physical size of the transceiver can undoubtedly increase the EDoF performance. For instance, the scenario with $L_t = L_r = 18\lambda$ can achieve about 89.4% EoF improvement compared with that of the scenario with $L_t = L_r = 15\lambda$. More importantly, when the physical size of the transceiver increases, the number of antennas, that achieves the approximated saturated EDoF performance, would also increase.

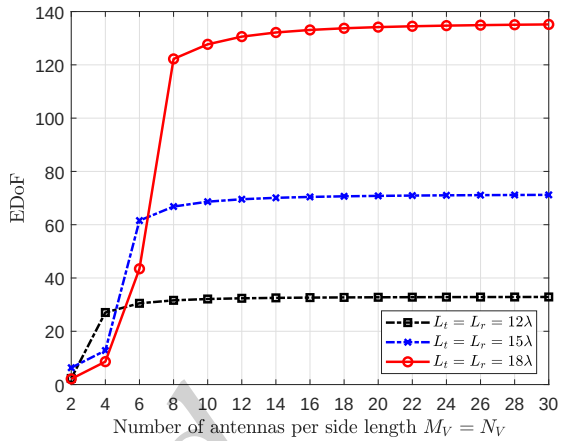

Fig. 2 EDoF performance for the UPA system over the dyadic Green channel against the number of antennas per side with different side length. We have $L_t = L_r$ and $D = 40\lambda$. EDoF, effective degree of freedom; UPA, uniform planar array.

Figure 3 analyzes the EDoF performance of the UPA system as a function of the number of antennas per side, considering different lengths of the receiving side. The figure reveals that for a fixed transmitting array aperture size, the EDoF performance benefits from a larger receiving array aperture size. For instance, about 94.4% EDoF improvement can be achieved for $L_r = 6\lambda$ compared with that of $L_r = 4\lambda$. Moreover, as the receiving array aperture size increases, the number of antennas required to achieve nearly optimal EDoF performance also increases.

In Fig. 4, we compare the EDoF performance

unedited

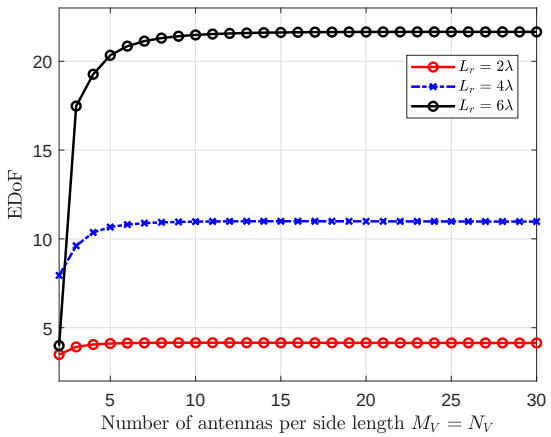

Fig. 3 EDoF performance for the UPA system against the number of antennas per side with different receiving side lengths over the dyadic Green channel. We have $L_t = 20\lambda$ and $D = 40\lambda$. EDoF, effective degree of freedom; UPA, uniform planar array.

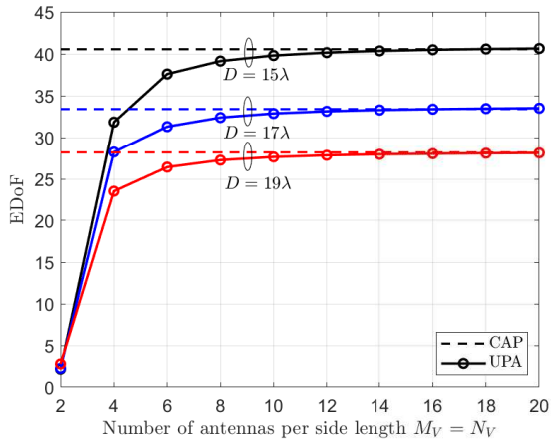

Fig. 4 EDoF performance for UPA system with $L_t = L_r = 8\lambda$ and 2D CAP plane system over the dyadic Green channel. EDoF, effective degree of freedom; UPA, uniform planar array; CAP, continuous aperture.

between the UPA and 2D CAP plane systems over the dyadic Green channel for various transmitting distances. As observed, with the number of antennas increasing, the EDoF performance of the UPA system initially increases and finally converges to that of the 2D CAP plane system. For the UPA system with a fixed physical size, increasing the number of antennas may not always improve the EDoF performance, where an approximately saturated EDoF performance can be achieved under a particular number of antennas. For instance, for $D = 15\lambda$, only 0.22% EDoF performance improvement can be achieved for $N_t = 18$ compared with that of $N_t = 16$; it is costly to increase the total of 68 antennas to achieve only a relatively small EDoF performance improvement. Thus, it is crucial to design the UPA system with the proper number of antennas to achieve nearly optimal EDoF performance.

Figure 5 considers the EDoF for the 2D CAP plane system as a function of transmitting distance D over different numbers of polarization. Note that the triple, double, and single polarization scenarios represent all three of the polarization directions, considering only the x and y polarization directions, and only the x polarization direction for the transceiver, respectively. As observed, the near-field with Green's function based-channel can significantly enhance the EDoF performance compared to the far-field with only 1 EDoF. The consideration of more polarization directions can improve the EDoF performance, for example 109.8% and 93.85% EDoF improvement can be achieved for the triple polarization scenario for $D = 4$ m compared with that of the double polarization and single polarization scenarios, respectively, because more EM waves can be impinged from different polarization directions. Additionally, with the increase of D, the performance gap between the triple and double polarization scenarios becomes smaller because z polarization vanishes with the transmitting distance increasing.

In Fig. 6, we evaluate the effect of the physical size of the 2D CAP plane system on the EDoF performance. It is found that the EDoF benefits from a larger physical size of both the transmitter and the receiver. For instance, for $L_r = 15\lambda$, 27.6% EDoF improvement can be achieved for the scenario with $L_t = 20\lambda$ compared with that of the scenario with $L_t = 15\lambda$. For the scenario with $L_t = 15\lambda$, the scenario with $L_r = 20\lambda$ can achieve 14.69% EDoF improvement compared with that of the scenario with $L_r = 15\lambda$. However, for a fixed value of L_t or L_r, the improvement rate of the EDoF performance would decrease with increasing L_r or L_t, because the EDoF performance is constrained by the smaller one between the physical sizes of the transmitter and the receiver. A similar argument is widely established in existing works, such as Tse and Viswanath (2005), which states that for discrete arrays, the DoF is limited by the lesser of the numbers of transmitting and receiving antennas. However, the similar conclusion for the near-field based CAP system above is motivated by the numerical results without detailed proof

unedited

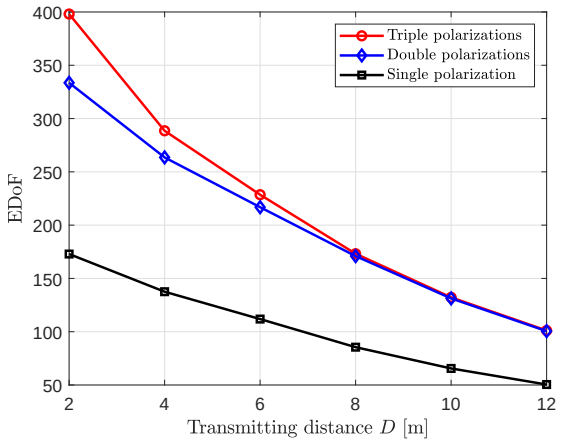

Fig. 5 EDoF performance against the transmitting distance D for the 2D CAP plane system over the dyadic Green channel with different numbers of polarization with $L_t = L_r = 30\lambda$. EDoF, effective degree of freedom; CAP, continuous aperture.

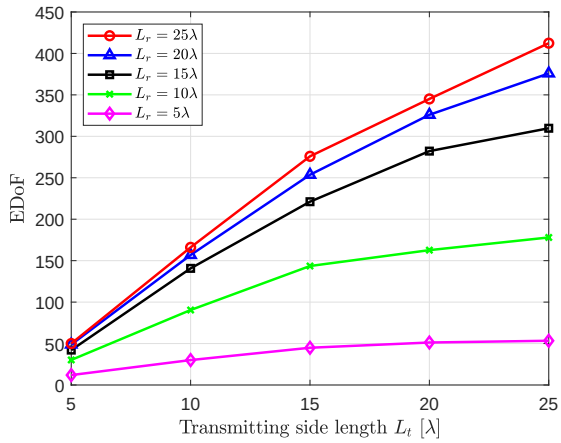

Fig. 6 EDoF performance against the side length of the 2D CAP plane transmitter L_t over the dyadic Green channel with different values of the side length of the 2D CAP plane receiver and $D = 13\lambda$. EDoF, effective degree of freedom; CAP, continuous aperture.

steps. Therefore, a comprehensive proof of this conclusion remains a necessary focus and a promising direction for future studies.

5 Conclusions

In this study, we investigated the EDoF performance analysis for the UPA and the 2D CAP systems. More importantly, the scalar and the dyadic Green near-field channels were considered. First, we derived the EDoF performance for the UPA system by utilizing discrete channel matrices based on either the scalar or dyadic Green's functions. For the 2D CAP plane system, the asymptotic analysis was applied to construct the EDoF performance analysis framework based on the scalar or dyadic Green channels. For the numerical results, we presented a comparative analysis of the EDoF performance between the UPA-based and 2D CAP plane-based XL-MIMO systems. Besides, we analyzed the effect of the polarization and the physical sizes of the transceiver. It was observed that, with an increasing number of antennas, the EDoF performance for the UPA system would approach that of the 2D CAP plane system. Moreover, the EDoF performance benefits from the polarization and the physical sizes of the transceiver. Future studies are anticipated to further explore the EDoF analysis for three-dimensional antenna array structures in XL-MIMO systems as in Yuan et al. (2024).

unedited

Contributors

Zhe WANG and Jiayi ZHANG designed the research. Wenhui YI processed the data. Zhe WANG drafted the manuscript. Huahua XIAO and Dusit Niyato helped organize the manuscript. Jiayi ZHANG, Dusit Niyato, and Bo AI revised and finalized the paper.

Conflict of interest

All the authors declare that they have no conflict of interest.

References

Arnoldus HF, 2001. Representation of the near-field, middle-field, and far-field electromagnetic green's functions in reciprocal space. *J Opt Soc Am B*, 18(4):547-555. https://doi.org/10.1364/JOSAB.18.000547

Björnson E, Sanguinetti L, Wymeersch H, et al., 2019. Massive MIMO is a realityâĂŤwhat is next?: Five promising research directions for antenna arrays. *Digital Signal Process*, 94:3-20. https://doi.org/10.1016/j.dsp.2019.06.007

Björnson E, Chae CB, Heath RW. J, et al., 2024. Towards 6G MIMO: Massive spatial multiplexing, dense arrays, and interplay between electromagnetics and processing, . https://doi.org/10.48550/arXiv.2401.02844

Chen SF, Zhang JY, Björnson E, et al., 2021. Structured massive access for scalable cell-free massive MIMO systems. *IEEE J Sel Areas Commun*, 39(4):1086-1100. https://doi.org/10.1109/JSAC.2020.3018836

Chen SF, Zhang JY, BjÃűrnson E, et al., 2023. Energy-efficient cell-free massive MIMO through sparse large-scale fading processing. *IEEE Trans Wirel Commun*, 22(12):9374-9389. https://doi.org/10.1109/TWC.2023.3270299

Cui MY, Dai LL, 2022. Channel estimation for extremely large-scale MIMO: Far-field or near-field? *IEEE Trans Commun*, 70(4):2663-2677.
https://doi.org/10.1109/TCOMM.2022.3146400

Cui MY, Wu ZD, Lu Y, et al., 2023. Near-field MIMO communications for 6G: Fundamentals, challenges, potentials, and future directions. *IEEE Commun Mag*, 61(1):40-46.
https://doi.org/10.1109/MCOM.004.2200136

Du HY, Wang JC, Niyato D, et al., 2023. Semantic communications for wireless sensing: RIS-aided encoding and self-supervised decoding. *IEEE J Sel Areas Commun*, 41(8):2547-2562.
https://doi.org/10.1109/JSAC.2023.3288231

Du HY, Zhang RC, Liu YQ, et al., 2024. Enhancing deep reinforcement learning: A tutorial on generative diffusion models in network optimization. *IEEE Commun Surv Tut*, in press.
https://doi.org/10.1109/COMST.2024.3400011

Gan X, Zhong CJ, Huang CW, et al., 2021. RIS-assisted multi-user MISO communications exploiting statistical CSI. *IEEE Trans Commun*, 69(10):6781-6792.
https://doi.org/10.1109/TCOMM.2021.3100860

Gong TR, Gavriilidis P, Ji R, et al., 2024. Holographic MIMO communications: Theoretical foundations, enabling technologies, and future directions. *IEEE Commun Surv Tut*, 26(1):196-257.
https://doi.org/10.1109/COMST.2023.3309529

Huang CW, Yang ZH, Alexandropoulos GC, et al., 2021. Multi-hop RIS-empowered terahertz communications: A DRL-based hybrid beamforming design. *IEEE J Sel Areas Commun*, 39(6):1663-1677.
https://doi.org/10.1109/JSAC.2021.3071836

Jiang YH, Gao FF, 2023. Electromagnetic channel model for near field MIMO systems in the half space. *IEEE Commun Lett*, 27(2):706-710.
https://doi.org/10.1109/LCOMM.2022.3229445

Lei H, Zhang JY, Wang Z, et al., 2024a. Hybrid-field channel estimation for XL-MIMO systems with stochastic gradient pursuit algorithm. *IEEE Trans Signal Process*, 72:2998-3012.
https://doi.org/10.1109/TSP.2024.3406348

Lei H, Zhang JY, Xiao HH, et al., 2024b. Channel estimation for XL-MIMO systems with polar-domain multi-scale residual dense network. *IEEE Trans Veh Technol*, 73(1):1479-1484.
https://doi.org/10.1109/TVT.2023.3311010

Letaief KB, Chen W, Shi YM, et al., 2019. The roadmap to 6G: AI empowered wireless networks. *IEEE Commun Mag*, 57(8):84-90.
https://doi.org/10.1109/MCOM.2019.1900271

Liu YW, Ouyang CJ, Wang ZL, et al., 2024. Near-field communications: A comprehensive survey, .
https://doi.org/10.48550/arXiv.2401.05900

Liu ZL, Zhang JY, Liu ZH, et al., 2024a. Cell-free XL-MIMO meets multi-agent reinforcement learning: Architectures, challenges, and future directions. *IEEE Wirel Commun*, in press.
https://doi.org/10.1109/MWC.007.2300176

Liu ZH, Zhang JY, Li ZL, et al., 2024b. Joint cooperative clustering and power control for energy-efficient cell-free XL-MIMO with multi-agent reinforcement learning. *IEEE Trans Commun*, in press.
https://doi.org/10.1109/TCOMM.2024.3415596

Liu ZH, Zhang JY, Liu ZL, et al., 2024c. Double-layer power control for mobile cell-free XL-MIMO with multi-agent reinforcement learning. *IEEE Trans Wirel Commun*, 23(5):4659-4674.
https://doi.org/10.1109/TWC.2023.3321334

Lu HQ, Zeng Y, 2022. Communicating with extremely large-scale array/surface: Unified modeling and performance analysis. *IEEE Trans Wirel Commun*, 21(6):4039-4053.
https://doi.org/10.1109/TWC.2021.3126384

Lu HQ, Zeng Y, You CS, et al., 2024. A tutorial on near-field XL-MIMO communications towards 6G. *IEEE Commun Surv Tut*, in press.
https://doi.org/10.1109/COMST.2024.3387749

Marzetta TL, 2010. Noncooperative cellular wireless with unlimited numbers of base station antennas. *IEEE Trans Wirel Commun*, 9(11):3590-3600.
https://doi.org/10.1109/TWC.2010.092810.091092

Ouyang CJ, Liu YW, Yang HW, 2022. Performance of downlink and uplink integrated sensing and communications (ISAC) systems. *IEEE Wirel Commun Lett*, 11(9):1850-1854.
https://doi.org/10.1109/LWC.2022.3184409

Ouyang CJ, Liu YW, Zhang XQ, et al., 2023. Near-field communications: A degree-of-freedom perspective, .
https://doi.org/10.48550/arXiv.2401.05900

Shi EY, Zhang JY, Du HY, et al., 2024. RIS-aided cell-free massive MIMO systems for 6G: Fundamentals, system design, and applications. *Proc IEEE*, 112(4):331-364.
https://doi.org/10.1109/JPROC.2024.3404491

Sun G, He L, Sun ZM, et al., 2024. Joint task offloading and resource allocation in aerial-terrestrial UAV networks with edge and fog computing for post-disaster rescue. *IEEE Trans Mob Comput*, 23(9):8582-8600.
https://doi.org/10.1109/TMC.2024.3350886

Tataria H, Shafi M, Molisch AF, et al., 2021. 6G wireless systems: Vision, requirements, challenges, insights, and opportunities. *Proc IEEE*, 109(7):1166-1199.
https://doi.org/10.1109/JPROC.2021.3061701

Tse D, Viswanath P, 2005. Fundamentals of wireless communication. Cambridge university press, Cambridge, UK.

Wang Z, Zhang JY, Du HY, et al., 2024. Extremely Large-Scale MIMO: Fundamentals, Challenges, Solutions, and Future Directions. *IEEE Wirel Commun*, 31(3):117-124.
https://doi.org/10.1109/MWC.132.2200443

Wang Z, Zhang JY, Du HY, et al., 2024. A tutorial on extremely large-scale MIMO for 6G: Fundamentals, signal processing, and applications. *IEEE Commun Surv Tut*, in press.
https://doi.org/10.1109/COMST.2023.3349276

Wei L, Huang CW, Alexandropoulos GC, et al., 2023. Tri-polarized holographic MIMO surfaces for near-field communications: Channel modeling and precoding design. *IEEE Trans Wirel Commun*, 22(12):8828-8842.
https://doi.org/10.1109/TWC.2023.3266298

Xie ZY, Liu YW, Xu JQ, et al., 2023. Performance analysis for near-field MIMO: Discrete and continuous aperture antennas. *IEEE Wirel Commun Lett*, 12(12):2258-2262.
https://doi.org/10.1109/LWC.2023.3317492

unedited

Xu BK, Zhang JY, Li JX, et al., 2023. Jac-PCG based low-complexity precoding for extremely large-scale MIMO systems. *IEEE Trans Veh Technol*, 72(12):16811-16816. https://doi.org/10.1109/TVT.2023.3293546

Xu BK, Zhang JY, Du HY, et al., 2024. Resource allocation for near-field communications: Fundamentals, tools, and outlooks. *IEEE Wirel Commun*, in press. https://doi.org/10.1109/MWC.016.2300528

You CS, Zhang YP, Wu CY, et al., 2023. Near-field beam management for extremely large-scale array communications, . https://doi.org/10.48550/arXiv.2306.16206

You XH, Wang CX, Huang J, et al., 2021. Towards 6G wireless communication networks: Vision, enabling technologies, and new paradigm shifts. *Sci China Inf Sci*, 64(1):110301. https://doi.org/10.1007/s11432-020-2955-6

Yuan SSA, He Z, Chen XM, et al., 2022. Electromagnetic effective degree of freedom of an MIMO system in free space. *IEEE Antennas Wirel Propag Lett*, 21(3):446-450. https://doi.org/10.1109/LAWP.2021.3135018

Yuan SS, Wu J, Xu HJ, et al., 2024. Breaking the degrees-of-freedom limit of holographic MIMO communications: A 3-D antenna array topology. *IEEE Trans Veh Technol*, 73(8):11276-11288. https://doi.org/10.1109/TVT.2024.3372704

Zhang JY, Björnson E, Matthaiou M, et al., 2020. Prospective multiple antenna technologies for beyond 5G. *IEEE J Sel Areas Commun*, 38(8):1637-1660. https://doi.org/10.1109/JSAC.2020.3000826

Zhang JY, Zhang J, Björnson E, et al., 2021a. Local partial zero-forcing combining for cell-free massive MIMO systems. *IEEE Trans Commun*, 69(12):8459-8473. https://doi.org/10.1109/TCOMM.2021.3110214

Zhang JY, Zhang J, Ng DWK, et al., 2021b. Improving sum-rate of cell-free massive MIMO with expanded compute-and-forward. *IEEE Trans Signal Process*, 70:202-215. https://doi.org/10.1109/TSP.2021.3129337

Zhang JY, Zhang J, Ng DWK, et al., 2023. Federated learning-based cell-free massive MIMO system for privacy-preserving. *IEEE Trans Wirel Commun*, 22(7):4449-4460. https://doi.org/10.1109/TWC.2022.3225812

Zhang ZJ, Dai LL, 2023. Pattern-division multiplexing for multi-user continuous-aperture MIMO. *IEEE J Sel Areas Commun*, 41(8):2350-2366. https://doi.org/10.1109/JSAC.2023.3288244

Zheng JK, Zhang JY, Cheng JL, et al., 2023. Asynchronous cell-free massive MIMO with rate-splitting. *IEEE J Sel Areas Commun*, 41(5):1366-1382. https://doi.org/10.1109/JSAC.2023.3240709

unedited